BULLETIN OF THE POLISH ACADEMY OF SCIENCES
TECHNICAL SCIENCES, Vol. 72(3), 2024, Article number: e149179
DOI: 10.24425/bpasts.2024.149179

Varying coefficients in parallel shared-memory variational splitting solvers for non-stationary Maxwell equations

Marcin ŁOŚ, Maciej WOŹNIAK, and Maciej PASZYŃSKI*

AGH University of Krakow, al. Mickiewicza 30, 30-059 Krakow, Poland

Abstract. Direction-splitting implicit solvers employ the regular structure of the computational domain augmented with the splitting of the partial differential operator to deliver linear computational cost solvers for time-dependent simulations. The finite difference community originally employed this method to deliver fast solvers for PDE-based formulations. Later, this method was generalized into so-called variational splitting. The tensor product structure of basis functions over regular computational meshes allows us to employ the Kronecker product structure of the matrix and obtain linear computational cost factorization for finite element method simulations. These solvers are traditionally used for fast simulations over the structures preserving the tensor product regularity. Their applications are limited to regular problems and regular model parameters. This paper presents a generalization of the method to deal with non-regular material data in the variational splitting method. Namely, we can vary the material data with test functions to obtain a linear computational cost solver over a tensor product grid with non-regular material data. Furthermore, as described by the Maxwell equations, we show how to incorporate this method into finite element method simulations of non-stationary electromagnetic wave propagation over the human head with material data based on the three-dimensional MRI scan.

Keywords: partial differential equations; finite element method; Maxwell equations; variational splitting; MRI scan data.

1. INTRODUCTION

The alternating directions method solver was originally proposed for finite difference implicit simulations [3,4]. The method delivers solutions to time-dependent problems in linear computational cost. This alternating directions method has been applied to the non-stationary Maxwell problem in the context of the finite difference method [1, 8]. As shown in [10–13], the alternating direction solver can also be applied to the variational form employed by the finite element method computations. It uses tensor product grids and higher order and continuity B-spline basis from the isogeometric analysis [2]. These variational splitting solvers based on the tensor products, as detailed in [10–13] also allow for linear computational cost higher-order and continuity time-dependent simulations.

Namely, for the mass matrix $\mathcal{M}$ we can decompose the matrix into the Kronecker product of two (in 2D) or three (in 3D) one-dimensional mass matrices $\mathcal{M}^x \otimes \mathcal{M}^y$

$$\begin{aligned}\mathcal{M} &= (B_{ij}, B_{kl})_{L^2} = \int_\Omega B_{ij} B_{kl}\, \mathrm{d}\Omega \\ &= \int_\Omega B_i^x(x) B_j^y(y) B_k^x(x) B_l^y(y)\, \mathrm{d}\Omega = \int_\Omega (B_i B_k)(x)\,(B_j B_l)(y)\, \mathrm{d}\Omega \\ &= \left(\int_{\Omega_x} B_i B_k\, \mathrm{d}x\right)\left(\int_{\Omega_y} B_j B_l\, \mathrm{d}y\right) = \mathcal{M}^x \otimes \mathcal{M}^y. \end{aligned} \tag{1}$$

For the stiffness matrix the splitting is not possible

$$\begin{aligned}\mathcal{S} &= \int_\Omega \frac{\partial B_i^x}{\partial x} B_j^y \frac{\partial B_k^x}{\partial x} B_l^y + B_i^x \frac{\partial B_j^y}{\partial y} B_k^x \frac{\partial B_l^y}{\partial y}\, \mathrm{d}\Omega \\ &= \int_{\Omega_x} \frac{\partial B_i}{\partial x}\frac{\partial B_k}{\partial x}\, \mathrm{d}x \int_{\Omega_y} B_j B_l\, \mathrm{d}y + \int_{\Omega_x} B_i B_k\, \mathrm{d}x \int_{\Omega_y} \frac{\partial B_j}{\partial y}\frac{\partial B_l}{\partial y}\, \mathrm{d}y \\ &= \mathcal{S}^x \otimes \mathcal{M}^y + \mathcal{M}^x \otimes \mathcal{S}^y \end{aligned} \tag{2}$$

but the implicit time integration schemes suitable for direction splitting [5–7], they mix the mass matrices with stiffness matrices and introduce sub-steps, e.g.

$$\mathcal{S}^x \otimes \mathcal{M}^y u^{k+1/2} = \mathcal{M}^x \otimes \mathcal{S}^y u^k, \tag{3}$$

$$\mathcal{M}^x \otimes \mathcal{S}^y u^{k+1} = \mathcal{S}^x \otimes \mathcal{M}^y u^{k+1/2} \tag{4}$$

The problem with is that material data coefficient must also preserve the Kronecker product structure, and thus application of this scheme on arbitrary structure is not possible. Petar Minev [9] introduced the alternating direction solver in the context of the finite difference method allowing for local varying of material data while preserving the linear computational cost of the solver. We show that the linear cost of the variational splitting solver and the method stability is also preserved for the finite element method. We show that we can vary arbitrary material data coefficients with test functions. In this paper we employ the implicit time integration scheme with variational splitting for the non-stationary Maxwell equations [14]. We design our solver for electromagnetic wave propagations in non-regular biological tissues, and we utilize the MRI scan of the human head

*e-mail: paszynsk@agh.edu.pl

Manuscript submitted 2023-08-05, revised 2023-12-30, initially accepted for publication 2024-01-29, published in May 2024.

to illustrate the concept. In this paper, we do not focus on the interpretation of the numerical results and detailed design of the electromagnetic wave antennas since this is a challenging problem itself. We instead present the method for incorporating non-regular material data, and we test it on a simple model problem. We implement the Maxwell solver in the parallel shared-memory IGA-ADS code [15]. We verify the computational cost of the solver using non-linear material data with scalability experiments. The novelty of our paper with respect to [14] is the introduction of the method allowing for changing the material data with test functions.

The structure of the paper is the following. In Section 2, we describe the idea of the varying coefficient in the alternating direction solver. Section 3 presents the strong and weak formulations of the non-stationary Maxwell equations with non-constant coefficients. Section 4 is devoted to numerical experiments, the manufactured solution problem, and the problem of propagation of EM waves over the human head. Section 5 presents the scalability measurements of the parallel code.

2. VARYING COEFFICIENTS IN ALTERNATING DIRECTIONS SOLVER

We show that varying material data with test functions do not alter the linear computational cost of the direction-splitting algorithm. To focus our attention, we derive 2D heat transfer,

$$\frac{\partial u}{\partial t} - \nabla\left(\varepsilon \nabla u\right) = f; \tag{5}$$

where we discretize the time derivative $\frac{\partial u}{\partial t} \approx \frac{u^{n+1}-u^n}{\tau}$ to obtain the weak formulation

$$\left(u^{n+1}, v\right) + \tau\left(\varepsilon \nabla u^{n+1}, \nabla v\right) = \left(\tau f + u^n, v\right) \forall v \tag{6}$$

We discretize with B-splines

$$u^{n+1} \approx u^{n+1}_{i,j} B^x_i B^y_j; \quad u^0 \approx u^0_{i,j} B^x_i B^y_j; \quad v = B^x_k B^y_l \tag{7}$$

to obtain the equations of the left-hand side of the weak form, one for each test function B^x_k, B^y_k. We assume that the material data $\varepsilon_{k,l}$ varies with test functions.

$$\text{LHS} = \sum_{i,j}\left(\int B^x_i B^y_j B^x_k B^y_l + \int \varepsilon_{k,l} \partial_x B^x_i B^y_j \partial_x B^x_k B^y_l + \int \varepsilon_{k,l} B^x_i \partial_y B^y_j B^x_k \partial_y B^y_l\right) u^{n+1}_{i,j} \quad \forall k,l \tag{8}$$

and the right-hand side terms, one for each test function $B^x_k B^y_l$

$$\text{RHS} = \sum_{i,j}\left(\int \tau f B^x_k B^y_l + \int B^x_i B^y_j B^x_k B^y_l\right) u^0_{i,j} \quad \forall k,l. \tag{9}$$

We separate directions on the left-hand-side

$$\text{LHS} = \sum_{i,j}\left(\int_x B^x_i B^x_k \int_y B^y_j B^y_l + \tau \int_x \partial_x B^x_i \partial_x B^x_k \int_y \varepsilon_{k,l} B^y_j B^y_l + \tau \int_x B^x_i B^x_k \int_y \varepsilon_{k,l} \partial_y B^y_j \partial_y B^y_l\right) u^{n+1}_{i,j} \quad \forall k,l. \tag{10}$$

We consider the following approximation of the left-hand side

$$\begin{aligned}
&\sum_{i,j}\left(\int_x B^x_i B^x_k + \tau\varepsilon_{k,l}\int_x \partial_x B^x_i \partial_x B^x_k\right)\left(\int_y B^y_j B^y_l + \tau\varepsilon_{k,l}\int_y \partial_y B^y_j \partial_y B^y_l\right) u^{n+1}_{i,j} \\
&= \sum_{i,j}\left[\int_x B^x_i B^x_k \int_y B^y_j B^y_l + \int_x B^x_i B^x_k \tau \int_y \varepsilon_{k,l} \partial_y B^y_j \partial_y B^y_l + \tau \int_x \partial_x B^x_i \partial_x B^x_k \int_y \varepsilon_{k,l} B^y_j B^y_l + \tau^2\varepsilon^2 \int_x \partial_x B^x_i \partial_x B^x_k \int_y \varepsilon_{k,l} \partial_y B^y_j \partial_y B^y_l\right] u^{n+1}_{i,j} \\
&\approx \sum_{i,j}\left[\int_x B^x_i B^x_k \int_y B^y_j B^y_l + \tau\varepsilon_{k,l}\int_x B^x_i B^x_k \int_y \partial_y B^y_j \partial_y B^y_l + \tau\varepsilon_{k,l}\int_x \partial_x B^x_i \partial_x B^x_k \int_y B^y_j B^y_l\right] u^{n+1}_{i,j} = \text{LHS} \quad \forall k,l.
\end{aligned} \tag{11}$$

We consider a linear B-splines over 2D mesh, presented in Fig. 1. The basis is defined as a tensor product of two-knot vectors $[0\ 0\ 1\ 2\ 2] \times [0\ 0\ 1\ 2\ 2]$.

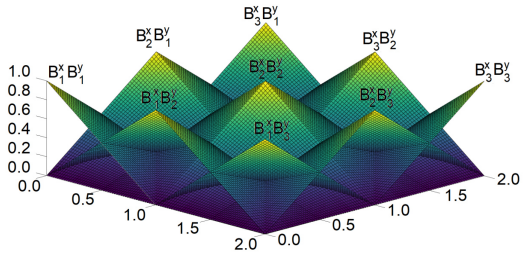

Fig. 1. 2D linear B-splines defined by $[0\ 0\ 1\ 2\ 2] \times [0\ 0\ 1\ 2\ 2]$

In this simple example, we employ linear B-splines. Thus some matrix entries are equal to zero (the integrals involve multiplications of B-splines that do not have common support). We do not cancel out the terms that are equal to zero to illustrate the global structure of the matrix. Instead, we denote by colors

the repeating terms in each of the blocks. Due to the size of the matrix, we print each row in a few lines.

$$\mathscr{A} = \begin{bmatrix}
\left(\int_x B^x B^x + \tau\varepsilon_{1,1}\int_x \partial_x B^x \partial_x B^x\right)\left(\int_y B_1^y B_1^y + \tau\varepsilon_{1,1}\int_y \partial_y B_1^y \partial_y B_1^y\right)\cdots \\
\cdots\left(\int_x B^z B^x + \tau\varepsilon_{1,1}\int_x \partial_x B^z \partial_x B^x\right)\left(\int_y B_1^y B_1^y + \tau\varepsilon_{1,1}\int_y \partial_y B_1^y \partial_y B_1^y\right)\cdots \\
\cdots\left(\int_x B^x B^x + \tau\varepsilon_{1,1}\int_x \partial_x B^x \partial_x B^x\right)\left(\int_y B_3^y B_1^y + \tau\varepsilon_{1,1}\int_y \partial_y B_3^y \partial_y B_1^y\right)\cdots \\
\cdots\left(\int_x B^z B^x + \tau\varepsilon_{1,1}\int_x \partial_x B^z \partial_x B^x\right)\left(\int_y B_3^y B_1^y + \tau\varepsilon_{1,1}\int_y \partial_y B_3^y \partial_y B_1^y\right) \\
\vdots\ \vdots\ \vdots \\
\left(\int_x B^x B^z + \tau\varepsilon_{3,1}\int_x \partial_x B^x \partial_x B^z\right)\left(\int_y B_1^y B_1^y + \tau\varepsilon_{3,1}\int_y \partial_y B_1^y \partial_y B_1^y\right)\cdots \\
\cdots\left(\int_x B^z B^z + \tau\varepsilon_{3,1}\int_x \partial_x B^z \partial_x B^z\right)\left(\int_y B_1^y B_1^y + \tau\varepsilon_{3,1}\int_y \partial_y B_1^y \partial_y B_1^y\right)\cdots \\
\cdots\left(\int_x B^x B^z + \tau\varepsilon_{3,1}\int_x \partial_x B^x \partial_x B^z\right)\left(\int_y B_3^y B_1^y + \tau\varepsilon_{3,1}\int_y \partial_y B_3^y \partial_y B_1^y\right)\cdots \\
\cdots\left(\int_x B^z B^z + \tau\varepsilon_{3,1}\int_x \partial_x B^z \partial_x B^z\right)\left(\int_y B_3^y B_1^y + \tau\varepsilon_{3,1}\int_y \partial_y B_3^y \partial_y B_1^y\right) \\
\vdots\ \vdots\ \vdots \\
\vdots\ \vdots\ \vdots \\
\left(\int_x B^x B^x + \tau\varepsilon_{1,3}\int_x \partial_x B^x \partial_x B^x\right)\left(\int_y B_1^y B_3^y + \tau\varepsilon_{1,3}\int_y \partial_y B_1^y \partial_y B_3^y\right)\cdots \\
\cdots\left(\int_x B^z B^x + \tau\varepsilon_{1,3}\int_x \partial_x B^z \partial_x B^x\right)\left(\int_y B_1^y B_3^y + \tau\varepsilon_{1,3}\int_y \partial_y B_1^y \partial_y B_3^y\right)\cdots \\
\cdots\left(\int_x B^x B^x + \tau\varepsilon_{1,3}\int_x \partial_x B^x \partial_x B^x\right)\left(\int_y B_3^y B_3^y + \tau\varepsilon_{1,3}\int_y \partial_y B_3^y \partial_y B_3^y\right)\cdots \\
\cdots\left(\int_x B^z B^x + \tau\varepsilon_{1,3}\int_x \partial_x B^z \partial_x B^x\right)\left(\int_y B_3^y B_3^y + \tau\varepsilon_{1,3}\int_y \partial_y B_3^y \partial_y B_3^y\right) \\
\vdots\ \vdots\ \vdots \\
\left(\int_x B^x B^z + \tau\varepsilon_{3,3}\int_x \partial_x B^x \partial_x B^z\right)\left(\int_y B_1^y B_3^y + \tau\varepsilon_{3,3}\int_y \partial_y B_1^y \partial_y B_3^y\right)\cdots \\
\cdots\left(\int_x B^z B^z + \tau\varepsilon_{3,3}\int_x \partial_x B^z \partial_x B^z\right)\left(\int_y B_1^y B_3^y + \tau\varepsilon_{3,3}\int_y \partial_y B_1^y \partial_y B_3^y\right)\cdots \\
\cdots\left(\int_x B^x B^z + \tau\varepsilon_{3,3}\int_x \partial_x B^x \partial_x B^z\right)\left(\int_y B_3^y B_3^y + \tau\varepsilon_{3,3}\int_y \partial_y B_3^y \partial_y B_3^y\right)\cdots \\
\cdots\left(\int_x B^z B^z + \tau\varepsilon_{3,3}\int_x \partial_x B^z \partial_x B^z\right)\left(\int_y B_3^y B_3^y + \tau\varepsilon_{3,3}\int_y \partial_y B_3^y \partial_y B_3^y\right)
\end{bmatrix}, \tag{12}$$

where the whole system is

$$\mathscr{A}\begin{bmatrix} u_{1,1} \\ \vdots \\ u_{3,3}\end{bmatrix} = \begin{bmatrix} \int F(x,y) B_{1,1}(x) B_{1,1}(y)\,\mathrm{d}x\,\mathrm{d}y \\ \vdots \\ \int F(x,y) B_{3,3}(x) B_{3,3}(y)\,\mathrm{d}x\,\mathrm{d}y\end{bmatrix}. \tag{13}$$

Note that each of the nine blocks (denoted by different colors) have a repeated matrix

$$\mathscr{A}_k = \begin{bmatrix}
\left(\int_x B^x B^x + \tau\varepsilon_{1,k}\int_x \partial_x B^x \partial_x B^x\right)\cdots\left(\int_x B^z B^x + \tau\varepsilon_{1,k}\int_x \partial_x B^z \partial_x B^x\right) \\
\cdots\vdots\cdots \\
\left(\int_x B^x B^z + \tau\varepsilon_{3,k}\int_x \partial_x B^x \partial_x B^z\right)\cdots\left(\int_x B^z B^z + \tau\varepsilon_{3,k}\int_x \partial_x B^z \partial_x B^z\right)
\end{bmatrix}. \tag{14}$$

We also define

$$\mathscr{B}_{1,k} = \begin{bmatrix}
\left(\int_y B_1^y B_k^y + \tau\varepsilon_{1,k}\int_y \partial_y B_1^y \partial_y B_k^y\right) & 0 & 0 \\
0 & \left(\int_y B_1^y B_k^y + \tau\varepsilon_{2,k}\int_y \partial_y B_1^y \partial_y B_k^y\right) & 0 \\
0 & 0 & \left(\int_y B_1^y B_k^y + \tau\varepsilon_{3,k}\int_y \partial_y B_1^y \partial_y B_k^y\right)
\end{bmatrix}, \tag{15}$$

$$\mathscr{B}_{2,k} = \begin{bmatrix}
\left(\int_y B_2^y B_k^y + \tau\varepsilon_{1,k}\int_y \partial_y B_2^y \partial_y B_k^y\right) & 0 & 0 \\
0 & \left(\int_y B_2^y B_k^y + \tau\varepsilon_{2,k}\int_y \partial_y B_2^y \partial_y B_k^y\right) & 0 \\
0 & 0 & \left(\int_y B_2^y B_k^y + \tau\varepsilon_{3,k}\int_y \partial_y B_2^y \partial_y B_k^y\right)
\end{bmatrix}, \tag{16}$$

$$\mathscr{B}_3, k = \begin{bmatrix}
\left(\int_y B_3^y B_k^y + \tau\varepsilon_{1,k}\int_y \partial_y B_3^y \partial_y B_k^y\right) & 0 & 0 \\
0 & \left(\int_y B_3^y B_k^y + \tau\varepsilon_{2,k}\int_y \partial_y B_3^y \partial_y B_k^y\right) & 0 \\
0 & 0 & \left(\int_y B_3^y B_k^y + \tau\varepsilon_{3,k}\int_y \partial_y B_3^y \partial_y B_k^y\right)
\end{bmatrix}. \tag{17}$$

We re-write our system as multiplication of two-matrices:

$$\begin{bmatrix} \mathscr{A}_1 & 0 & 0 \\ 0 & \mathscr{A}_2 & 0 \\ 0 & 0 & \mathscr{A}_3\end{bmatrix}\begin{bmatrix} \mathscr{B}_{1,1} & \mathscr{B}_{2,1} & \mathscr{B}_{3,1} \\ \mathscr{B}_{1,2} & \mathscr{B}_{2,2} & \mathscr{B}_{3,2} \\ \mathscr{B}_{1,3} & \mathscr{B}_{2,3} & \mathscr{B}_{3,3}\end{bmatrix}\begin{bmatrix} U_1 \\ \vdots \\ U_3\end{bmatrix} = \begin{bmatrix} \mathscr{F}_1 \\ \mathscr{F}_2 \\ \mathscr{F}_3\end{bmatrix},$$

$$\mathscr{F}_1 = \begin{bmatrix} \int F_{1,1}(x,y) B^x B_1^y \\ \int F_{1,2}(x,y) B^x B_2^y \\ \int F_{1,3}(x,y) B^x B_3^y\end{bmatrix}, \quad \mathscr{F}_2 = \begin{bmatrix} \int F_{2,1}(x,y) B^y B_1^y \\ \int F_{2,2}(x,y) B^y B_2^y \\ \int F_{2,3}(x,y) B^y B_3^y\end{bmatrix}, \tag{18}$$

$$\mathscr{F}_3 = \begin{bmatrix} \int F_{3,1}(x,y) B^z B_1^y \\ \int F_{3,2}(x,y) B^z B_2^y \\ \int F_{3,3}(x,y) B^z B_3^y\end{bmatrix}, \quad U_i = \begin{bmatrix} u_{i,1} \\ u_{i,2} \\ u_{i,3}\end{bmatrix}$$

and $F_{k,l} = \int \tau f B_k^x B_l^y + \int \sum B_i^x B_j^y u_{ij}^0 B_k^x B_l^y$. We define

$$\begin{bmatrix} \mathscr{G}_1 \\ \mathscr{G}_2 \\ \mathscr{G}_3 \end{bmatrix} = \begin{bmatrix} \mathscr{B}_{1,1} & \mathscr{B}_{2,1} & \mathscr{B}_{3,1} \\ \mathscr{B}_{1,2} & \mathscr{B}_{2,2} & \mathscr{B}_{3,2} \\ \mathscr{B}_{1,3} & \mathscr{B}_{2,3} & \mathscr{B}_{3,3} \end{bmatrix} \begin{bmatrix} U_1 \\ U_2 \\ U_3 \end{bmatrix}. \tag{19}$$

In our solver, we solve

$$\begin{bmatrix} \mathscr{A}_1 & 0 & 0 \\ 0 & \mathscr{A}_2 & 0 \\ 0 & 0 & \mathscr{A}_3 \end{bmatrix} \begin{bmatrix} \mathscr{G}_1 \\ \mathscr{G}_2 \\ \mathscr{G}_3 \end{bmatrix} = \begin{bmatrix} \mathscr{F}_1 \\ \mathscr{F}_2 \\ \mathscr{F}_3 \end{bmatrix}, \tag{20}$$

for $\mathscr{G}_1, \mathscr{G}_2, \mathscr{G}_3$, and then we solve

$$\begin{bmatrix} \mathscr{B}_{1,1} & \mathscr{B}_{2,1} & \mathscr{B}_{3,1} \\ \mathscr{B}_{1,2} & \mathscr{B}_{2,2} & \mathscr{B}_{3,2} \\ \mathscr{B}_{1,3} & \mathscr{B}_{2,3} & \mathscr{B}_{3,3} \end{bmatrix} \begin{bmatrix} U_1 \\ U_2 \\ U_3 \end{bmatrix} = \begin{bmatrix} \mathscr{G}_1 \\ \mathscr{G}_2 \\ \mathscr{G}_3 \end{bmatrix}. \tag{21}$$

Both systems (20)–(21) can be solved in a linear computational cost due to the banded structures of matrices build with one-dimensional B-splines.

3. VARIATIONAL SPLITTING WITH NON-REGULAR MATERIAL DATA FOR MAXWELL EQUATIONS

We utilize the alternating directions solver that delivers linear computational cost factorization on tensor product grids. The solver decomposes the system of linear equations related to the three-dimensional mesh into three multi-diagonal sub-systems related to one-dimensional grids with multiple right-hand sides. The non-regular material data can be embedded into the solver by local modifications to the rows and columns in the three sub-systems. Namely, we can change the material data corresponding to different equations, and these modifications do not break the solver linear computational cost. We verify this method by running the example of the propagation of electromagnetic waves on the human head. Petar Minev has proposed this method initially for finite difference simulations [9]. In the IGA context, the modification is not point-wise but rather test-function-wise since each equation in the global system is related to a single test function rather than a point in the stencil.

3.1. Time integration scheme allowing for direction splitting of Maxwell equations

Following [1,8] we employ the implicit time integration scheme allowing for splitting of the Maxwell equations:

$$\begin{aligned} \mathbf{E}^{n+\frac{1}{2}} &- \begin{bmatrix} \frac{\tau^2}{4\varepsilon}\frac{\partial}{\partial y}\mu^{-1}\frac{\partial}{\partial y} & 0 & 0 \\ 0 & \frac{\tau^2}{4\varepsilon}\frac{\partial}{\partial z}\mu^{-1}\frac{\partial}{\partial z} & 0 \\ 0 & 0 & \frac{\tau^2}{4\varepsilon}\frac{\partial}{\partial x}\mu^{-1}\frac{\partial}{\partial x} \end{bmatrix} \mathbf{E}^{n+\frac{1}{2}} \\ &= \mathbf{E}^n + \frac{\tau}{2\varepsilon}\begin{bmatrix} 0 & -\frac{\partial}{\partial z} & \frac{\partial}{\partial y} \\ \frac{\partial}{\partial z} & 0 & -\frac{\partial}{\partial x} \\ -\frac{\partial}{\partial y} & \frac{\partial}{\partial x} & 0 \end{bmatrix} \mathbf{H}^n \\ &- \frac{\tau^2}{4\varepsilon}\begin{bmatrix} 0 & \frac{\partial}{\partial y}\mu^{-1}\frac{\partial}{\partial x} & 0 \\ 0 & 0 & \frac{\partial}{\partial z}\mu^{-1}\frac{\partial}{\partial y} \\ \frac{\partial}{\partial x}\mu^{-1}\frac{\partial}{\partial z} & 0 & 0 \end{bmatrix} \mathbf{E}^n, \end{aligned} \tag{22}$$

$$\mathbf{H}^{n+\frac{1}{2}} = \mathbf{H}^n - \frac{\tau}{2\mu}\begin{bmatrix} 0 & 0 & \frac{\partial}{\partial y} \\ \frac{\partial}{\partial z} & 0 & 0 \\ 0 & \frac{\partial}{\partial x} & 0 \end{bmatrix} \mathbf{E}^n + \frac{\tau}{2\mu}\begin{bmatrix} 0 & \frac{\partial}{\partial z} & 0 \\ 0 & 0 & \frac{\partial}{\partial x} \\ \frac{\partial}{\partial y} & 0 & 0 \end{bmatrix} \mathbf{E}^{n+\frac{1}{2}}$$

$$\begin{aligned} \mathbf{E}^{n+1} &- \begin{bmatrix} \frac{\tau^2}{4\varepsilon}\frac{\partial}{\partial z}\mu^{-1}\frac{\partial}{\partial z} & 0 & 0 \\ 0 & \frac{\tau^2}{4\varepsilon}\frac{\partial}{\partial x}\mu^{-1}\frac{\partial}{\partial x} & 0 \\ 0 & 0 & \frac{\tau^2}{4\varepsilon}\frac{\partial}{\partial y}\mu^{-1}\frac{\partial}{\partial y} \end{bmatrix} \mathbf{E}^{n+1} \\ &= \mathbf{E}^{n+\frac{1}{2}} + \frac{\tau}{2\varepsilon}\begin{bmatrix} 0 & -\frac{\partial}{\partial z} & \frac{\partial}{\partial y} \\ \frac{\partial}{\partial z} & 0 & -\frac{\partial}{\partial x} \\ -\frac{\partial}{\partial y} & \frac{\partial}{\partial x} & 0 \end{bmatrix} \mathbf{H}^{n+\frac{1}{2}} \\ &- \frac{\tau^2}{4\varepsilon}\begin{bmatrix} 0 & 0 & \frac{\partial}{\partial z}\mu^{-1}\frac{\partial}{\partial x} \\ \frac{\partial}{\partial x}\mu^{-1}\frac{\partial}{\partial y} & 0 & 0 \\ 0 & \frac{\partial}{\partial y}\mu^{-1}\frac{\partial}{\partial z} & 0 \end{bmatrix} \mathbf{E}^{n+\frac{1}{2}}, \end{aligned} \tag{23}$$

$$\begin{aligned} \mathbf{H}^{n+1} &= \mathbf{H}^{n+\frac{1}{2}} \\ &+ \frac{\tau}{2\mu}\begin{bmatrix} 0 & \frac{\partial}{\partial z} & 0 \\ 0 & 0 & \frac{\partial}{\partial x} \\ \frac{\partial}{\partial y} & 0 & 0 \end{bmatrix} \mathbf{E}^{n+\frac{1}{2}} - \frac{\tau}{2\mu}\begin{bmatrix} 0 & 0 & \frac{\partial}{\partial y} \\ \frac{\partial}{\partial z} & 0 & 0 \\ 0 & \frac{\partial}{\partial x} & 0 \end{bmatrix} \mathbf{E}^{n+1}. \end{aligned}$$

3.2. Variational splitting for Maxwell equations

In this section, following [14], we derive the variational formulations for the time-integration schemes described in the previous section. We multiply by test functions (V_x, V_y, V_z) and integrate by parts

$$\begin{bmatrix} \left(E_x{}^{n+\frac{1}{2}}, V_x\right) \\ \left(E_y{}^{n+\frac{1}{2}}, V_y\right) \\ \left(E_z{}^{n+\frac{1}{2}}, V_z\right) \end{bmatrix} - \frac{\tau^2}{4\varepsilon}\begin{bmatrix} \left(\frac{\partial}{\partial y}\mu^{-1}\frac{\partial}{\partial y}E_x{}^{n+\frac{1}{2}}, V_x\right) \\ \left(\frac{\partial}{\partial z}\mu^{-1}\frac{\partial}{\partial z}E_y{}^{n+\frac{1}{2}}, V_y\right) \\ \left(\frac{\partial}{\partial x}\mu^{-1}\frac{\partial}{\partial x}E_z{}^{n+\frac{1}{2}}, V_z\right) \end{bmatrix} = \begin{bmatrix} (E_x{}^n, V_x) \\ (E_y{}^n, V_y) \\ (E_z{}^n, V_z) \end{bmatrix}$$

$$+\frac{\tau}{2\varepsilon}\begin{bmatrix} -\left(\frac{\partial}{\partial z}H_y{}^n, V_x\right) + \left(\frac{\partial}{\partial y}H_z{}^n, V_x\right) \\ \left(\frac{\partial}{\partial z}H_x{}^n, V_y\right) - \left(\frac{\partial}{\partial x}H_z{}^n, V_y\right) \\ -\left(\frac{\partial}{\partial y}H_x{}^n, V_z\right) + \left(\frac{\partial}{\partial x}H_y{}^n, V_z\right) \end{bmatrix} - \frac{\tau^2}{4\varepsilon}\begin{bmatrix} \left(\frac{\partial}{\partial y}\mu^{-1}\frac{\partial}{\partial x}E_y{}^n, V_x\right) \\ \left(\frac{\partial}{\partial y}\mu^{-1}\frac{\partial}{\partial z}E_z{}^n, V_y\right) \\ \left(\frac{\partial}{\partial x}\mu^{-1}\frac{\partial}{\partial z}E_x{}^n, V_z\right) \end{bmatrix}$$

$$\begin{bmatrix}\left(H_x{}^{n+\frac{1}{2}},V_x\right)\\ \left(H_y{}^{n+\frac{1}{2}},V_y\right)\\ \left(H_z{}^{n+\frac{1}{2}},V_z\right)\end{bmatrix}=\begin{bmatrix}(H_x{}^n,V_x)\\ (H_y{}^n,V_y)\\ (H_z{}^n,V_z)\end{bmatrix}-\frac{\tau}{2\mu}\begin{bmatrix}\left(\frac{\partial}{\partial y}E_z{}^n,V_x\right)\\ \left(\frac{\partial}{\partial z}E_x{}^n,V_y\right)\\ \left(\frac{\partial}{\partial x}E_y{}^n,V_z\right)\end{bmatrix} \tag{24}$$

$$+\frac{\tau}{2\mu}\begin{bmatrix}\left(\frac{\partial}{\partial z}E_y{}^{n+\frac{1}{2}},V_x\right)\\ \left(\frac{\partial}{\partial x}E_z{}^{n+\frac{1}{2}},V_y\right)\\ \left(\frac{\partial}{\partial y}E_x{}^{n+\frac{1}{2}},V_z\right)\end{bmatrix}$$

$$\begin{bmatrix}(E_x{}^{n+1},V_x)\\ (E_y{}^{n+1},V_y)\\ (E_z{}^{n+1},V_z)\end{bmatrix}-\frac{\tau^2}{4\varepsilon}\begin{bmatrix}\left(\frac{\partial}{\partial z}\mu^{-1}\frac{\partial}{\partial z}E_x{}^{n+1},V_x\right)\\ \left(\frac{\partial}{\partial x}\mu^{-1}\frac{\partial}{\partial x}E_y{}^{n+1},V_y\right)\\ \left(\frac{\partial}{\partial y}\mu^{-1}\frac{\partial}{\partial y}E_z{}^{n+1},V_z\right)\end{bmatrix}=\begin{bmatrix}\left(E_x{}^{n+\frac{1}{2}},V_x\right)\\ \left(E_y{}^{n+\frac{1}{2}},V_y\right)\\ \left(E_z{}^{n+\frac{1}{2}},V_z\right)\end{bmatrix}$$

$$+\frac{\tau}{2\varepsilon}\begin{bmatrix}-\left(\frac{\partial}{\partial z}H_y{}^{n+\frac{1}{2}},V_x\right)+\left(\frac{\partial}{\partial y}H_z{}^{n+\frac{1}{2}},V_x\right)\\ \left(\frac{\partial}{\partial z}H_x{}^{n+\frac{1}{2}},V_y\right)-\left(\frac{\partial}{\partial x}H_z{}^{n+\frac{1}{2}},V_y\right)\\ -\left(\frac{\partial}{\partial y}H_x{}^{n+\frac{1}{2}},V_z\right)+\left(\frac{\partial}{\partial x}H_y{}^{n+\frac{1}{2}},V_z\right)\end{bmatrix} \tag{25}$$

$$-\frac{\tau^2}{4\varepsilon}\begin{bmatrix}\left(\frac{\partial}{\partial x}\mu^{-1}\frac{\partial}{\partial z}E_z{}^{n+\frac{1}{2}},V_x\right)\\ \left(\frac{\partial}{\partial x}\mu^{-1}\frac{\partial}{\partial y}E_x{}^{n+\frac{1}{2}},V_y\right)\\ \left(\frac{\partial}{\partial y}\mu^{-1}\frac{\partial}{\partial z}E_y{}^{n+\frac{1}{2}},V_z\right)\end{bmatrix}$$

$$\begin{bmatrix}(H_x{}^{n+1},V_x)\\ (H_y{}^{n+1},V_y)\\ (H_z{}^{n+1},V_z)\end{bmatrix}=\begin{bmatrix}\left(H_x{}^{n+\frac{1}{2}},V_x\right)\\ \left(H_y{}^{n+\frac{1}{2}},V_y\right)\\ \left(H_z{}^{n+\frac{1}{2}},V_z\right)\end{bmatrix}-\frac{\tau}{2\mu}\begin{bmatrix}\left(\frac{\partial}{\partial z}E_y{}^{n+\frac{1}{2}},V_x\right)\\ \left(\frac{\partial}{\partial x}E_z{}^{n+\frac{1}{2}},V_y\right)\\ \left(\frac{\partial}{\partial y}E_x{}^{n+\frac{1}{2}},V_z\right)\end{bmatrix}$$
$$-\frac{\tau}{2\mu}\begin{bmatrix}\left(\frac{\partial}{\partial y}E_z{}^{n+1},V_x\right)\\ \left(\frac{\partial}{\partial z}E_x{}^{n+1},V_y\right)\\ \left(\frac{\partial}{\partial x}E_y{}^{n+1},V_z\right)\end{bmatrix}.$$

Integrating by parts, removing boundary terms, we obtain

$$\begin{bmatrix}\left(E_x{}^{n+\frac{1}{2}},V_x\right)\\ \left(E_y{}^{n+\frac{1}{2}},V_y\right)\\ \left(E_z{}^{n+\frac{1}{2}},V_z\right)\end{bmatrix}+\frac{\tau^2}{4\varepsilon\mu}\begin{bmatrix}\left(\frac{\partial}{\partial y}E_x{}^{n+\frac{1}{2}},\frac{\partial}{\partial y}V_x\right)\\ \left(\frac{\partial}{\partial z}E_y{}^{n+\frac{1}{2}},\frac{\partial}{\partial z}V_y\right)\\ \left(\frac{\partial}{\partial x}E_z{}^{n+\frac{1}{2}},\frac{\partial}{\partial x}V_z\right)\end{bmatrix}=$$
$$\begin{bmatrix}(E_x{}^n,V_x)\\ (E_y{}^n,V_y)\\ (E_z{}^n,V_z)\end{bmatrix}+\frac{\tau}{2\varepsilon}\begin{bmatrix}-\left(\frac{\partial}{\partial z}H_y{}^n,V_x\right)+\left(\frac{\partial}{\partial y}H_z{}^n,V_x\right)\\ \left(\frac{\partial}{\partial z}H_x{}^n,V^2\right)-\left(\frac{\partial}{\partial x}H_z{}^n,V_y\right)\\ -\left(\frac{\partial}{\partial y}H_x{}^n,V_z\right)+\left(\frac{\partial}{\partial x}H_y{}^n,V_z\right)\end{bmatrix}$$
$$+\frac{\tau^2}{4\varepsilon\mu}\begin{bmatrix}\left(\frac{\partial}{\partial x}E_y{}^n,\frac{\partial}{\partial y}V_x\right)\\ \left(\frac{\partial}{\partial z}E_z{}^n,\frac{\partial}{\partial y}V_y\right)\\ \left(\frac{\partial}{\partial z}E_x{}^n,\frac{\partial}{\partial x}V_z\right)\end{bmatrix} \tag{26}$$

$$\begin{bmatrix}\left(H_x{}^{n+\frac{1}{2}},V_x\right)\\ \left(H_y{}^{n+\frac{1}{2}},V_y\right)\\ \left(H_z{}^{n+\frac{1}{2}},V_z\right)\end{bmatrix}=\begin{bmatrix}(H_x{}^n,V_x)\\ (H_y{}^n,V_y)\\ (H_z{}^n,V_z)\end{bmatrix}-\frac{\tau}{2\mu}\begin{bmatrix}\left(\frac{\partial}{\partial y}E_z{}^n,V_x\right)\\ \left(\frac{\partial}{\partial z}E_x{}^n,V_y\right)\\ \left(\frac{\partial}{\partial x}E_y{}^n,V_z\right)\end{bmatrix}$$
$$+\frac{\tau}{2\mu}\begin{bmatrix}\left(\frac{\partial}{\partial z}E_y{}^{n+\frac{1}{2}},V_x\right)\\ \left(\frac{\partial}{\partial x}E_z{}^{n+\frac{1}{2}},V_y\right)\\ \left(\frac{\partial}{\partial y}E_x{}^{n+\frac{1}{2}},V_z\right)\end{bmatrix}$$

$$\begin{bmatrix}(E_x{}^{n+1},V_x)\\ (E_y{}^{n+1},V_y)\\ (E_z{}^{n+1},V_z)\end{bmatrix}+\frac{\tau^2}{4\varepsilon\mu}\begin{bmatrix}\left(\frac{\partial}{\partial z}E_x{}^{n+1},\frac{\partial}{\partial z}V_x\right)\\ \left(\frac{\partial}{\partial x}E_y{}^{n+1},\frac{\partial}{\partial x}V_y\right)\\ \left(\frac{\partial}{\partial y}E_z{}^{n+1},\frac{\partial}{\partial y}V_z\right)\end{bmatrix}=\begin{bmatrix}\left(E_x{}^{n+\frac{1}{2}},V_x\right)\\ \left(E_y{}^{n+\frac{1}{2}},V_y\right)\\ \left(E_z{}^{n+\frac{1}{2}},V_z\right)\end{bmatrix}$$

$$+\frac{\tau}{2\varepsilon}\begin{bmatrix}-\left(\frac{\partial}{\partial z}H_y{}^{n+\frac{1}{2}},V_x\right)+\left(\frac{\partial}{\partial y}H_z{}^{n+\frac{1}{2}},V_x\right)\\ \left(\frac{\partial}{\partial z}H_x{}^{n+\frac{1}{2}},V_y\right)-\left(\frac{\partial}{\partial x}H_z{}^{n+\frac{1}{2}},V_y\right)\\ -\left(\frac{\partial}{\partial y}H_x{}^{n+\frac{1}{2}},V_z\right)+\left(\frac{\partial}{\partial x}H_y{}^{n+\frac{1}{2}},V_z\right)\end{bmatrix} \tag{27}$$
$$-\frac{\tau^2}{4\varepsilon\mu}\begin{bmatrix}\left(\frac{\partial}{\partial z}E_z{}^{n+\frac{1}{2}},\frac{\partial}{\partial x}V_x\right)\\ \left(\frac{\partial}{\partial y}E_x{}^{n+\frac{1}{2}},\frac{\partial}{\partial x}V_y\right)\\ \left(\frac{\partial}{\partial z}E_y{}^{n+\frac{1}{2}},\frac{\partial}{\partial y}V_z\right)\end{bmatrix}$$

$$\begin{bmatrix}(H_x{}^{n+1},V_x)\\ (H_y{}^{n+1},V_y)\\ (H_z{}^{n+1},V_z)\end{bmatrix}=\begin{bmatrix}\left(H_x{}^{n+\frac{1}{2}},V_x\right)\\ \left(H_y{}^{n+\frac{1}{2}},V_y\right)\\ \left(H_z{}^{n+\frac{1}{2}},V_z\right)\end{bmatrix}-\frac{\tau}{2\mu}\begin{bmatrix}\left(\frac{\partial}{\partial z}E_y{}^{n+\frac{1}{2}},V_x\right)\\ \left(\frac{\partial}{\partial x}E_z{}^{n+\frac{1}{2}},V_y\right)\\ \left(\frac{\partial}{\partial y}E_x{}^{n+\frac{1}{2}},V_z\right)\end{bmatrix}$$
$$-\frac{\tau}{2\mu}\begin{bmatrix}\left(\frac{\partial}{\partial y}E_z{}^{n+1},V_x\right)\\ \left(\frac{\partial}{\partial z}E_x{}^{n+1},V_y\right)\\ \left(\frac{\partial}{\partial x}E_y{}^{n+1},V_z\right)\end{bmatrix}. \tag{28}$$

Expressing problem (26)–(28) in the matrix form we have

$$\begin{bmatrix}M_x\otimes M_y\otimes M_zE_x{}^{n+\frac{1}{2}}\\ M_x\otimes M_y\otimes M_zE_y{}^{n+\frac{1}{2}}\\ M_x\otimes M_y\otimes M_zE_z{}^{n+\frac{1}{2}}\end{bmatrix}+\frac{\tau^2}{4\varepsilon\mu}\begin{bmatrix}M_x\otimes S_y\otimes M_zE_x{}^{n+\frac{1}{2}}\\ M_x\otimes M_y\otimes S_zE_y{}^{n+\frac{1}{2}}\\ S_x\otimes M_y\otimes M_zE_z{}^{n+\frac{1}{2}}\end{bmatrix}$$
$$=\begin{bmatrix}M_x\otimes M_y\otimes M_zE_x{}^n\\ M_x\otimes M_y\otimes M_zE_y{}^n\\ M_x\otimes M_y\otimes M_zE_z{}^n\end{bmatrix}$$
$$+\frac{\tau}{2\varepsilon}\begin{bmatrix}-M_x\otimes M_y\otimes A_zH_y{}^n+M_x\otimes A_y\otimes M_zH_z{}^n\\ M_x\otimes M_y\otimes A_zH_x{}^n-A_x\otimes M_y\otimes M_zH_z{}^n\\ -M_x\otimes A_y\otimes M_zH_x{}^n+A_x\otimes M_y\otimes M_zH_y{}^n\end{bmatrix}$$
$$+\frac{\tau^2}{4\varepsilon\mu}\begin{bmatrix}A_x\otimes A_y\otimes M_zE_y{}^n\\ M_x\otimes A_y\otimes A_zE_z{}^n\\ A_x\otimes M_y\otimes M_zE_x{}^n\end{bmatrix}, \tag{29}$$

$$\begin{bmatrix} M_x \otimes M_y \otimes M_z H_x{}^{n+\frac{1}{2}} \\ M_x \otimes M_y \otimes M_z H_y{}^{n+\frac{1}{2}} \\ M_x \otimes M_y \otimes M_z H_z{}^{n+\frac{1}{2}} \end{bmatrix} = \begin{bmatrix} M_x \otimes M_y \otimes M_z H_x{}^{n} \\ M_x \otimes M_y \otimes M_z H_y{}^{n} \\ M_x \otimes M_y \otimes M_z H_z{}^{n} \end{bmatrix} - \frac{\tau}{2\mu} \begin{bmatrix} M_x \otimes A_y \otimes M_z E_z{}^{n} \\ M_x \otimes M_y \otimes A_z E_x{}^{n} \\ A_x \otimes M_y \otimes M_z E_y{}^{n} \end{bmatrix} + \frac{\tau}{2\mu} \begin{bmatrix} M_x \otimes M_y \otimes A_z E_y{}^{n+\frac{1}{2}} \\ A_x \otimes M_y \otimes M_z E_z{}^{n+\frac{1}{2}} \\ M_x \otimes M_A \otimes M_z E_x{}^{n+\frac{1}{2}} \end{bmatrix}, \tag{30}$$

$$\begin{bmatrix} M_x \otimes M_y \otimes M_z E_x{}^{n+1} \\ M_x \otimes M_y \otimes M_z E_y{}^{n+1} \\ M_x \otimes M_y \otimes M_z E_z{}^{n+1} \end{bmatrix} + \frac{\tau^2}{4\varepsilon\mu} \begin{bmatrix} M_x \otimes M_y \otimes S_z E_x{}^{n+1} \\ S_x \otimes M_y \otimes M_z E_y{}^{n+1} \\ M_x \otimes S_y \otimes M_z E_z{}^{n+1} \end{bmatrix} = \begin{bmatrix} M_x \otimes M_y \otimes M_z E_x{}^{n+\frac{1}{2}} \\ M_x \otimes M_y \otimes M_z E_y{}^{n+\frac{1}{2}} \\ M_x \otimes M_y \otimes M_z E_z{}^{n+\frac{1}{2}} \end{bmatrix} + \frac{\tau}{2\varepsilon} \begin{bmatrix} -M_x \otimes M_y \otimes A_z H_y{}^{n+\frac{1}{2}} + M_x \otimes A_y \otimes M_z H_z{}^{n+\frac{1}{2}} \\ M_x \otimes M_y \otimes A_z H_x{}^{n+\frac{1}{2}} - A_x \otimes M_y \otimes M_z H_z{}^{n+\frac{1}{2}} \\ -M_x \otimes A_y \otimes M_z H_x{}^{n+\frac{1}{2}} + A_x \otimes M_y \otimes M_z H_y{}^{n+\frac{1}{2}} \end{bmatrix} - \frac{\tau^2}{4\varepsilon\mu} \begin{bmatrix} A_x \otimes M_y \otimes A_z E_z{}^{n+\frac{1}{2}} \\ A_x \otimes A_y \otimes M_z E_x{}^{n+\frac{1}{2}} \\ M_x \otimes A_y \otimes A_z E_y{}^{n+\frac{1}{2}} \end{bmatrix} \tag{31}$$

$$\begin{bmatrix} M_x \otimes M_y \otimes M_z H_x{}^{n+1} \\ M_x \otimes M_y \otimes M_z H_y{}^{n+1} \\ M_x \otimes M_y \otimes M_z H_z{}^{n+1} \end{bmatrix} = \begin{bmatrix} M_x \otimes M_y \otimes M_z H_x{}^{n+\frac{1}{2}} \\ M_x \otimes M_y \otimes M_z H_y{}^{n+\frac{1}{2}} \\ M_x \otimes M_y \otimes M_z H_z{}^{n+\frac{1}{2}} \end{bmatrix} - \frac{\tau}{2\mu} \begin{bmatrix} M_x \otimes M_y \otimes A_z E_y{}^{n+\frac{1}{2}} \\ A_x \otimes M_y \otimes M_z E_z{}^{n+\frac{1}{2}} \\ M_x \otimes A_y \otimes M_z E_x{}^{n+\frac{1}{2}} \end{bmatrix} - \frac{\tau}{2\mu} \begin{bmatrix} M_x \otimes A_y \otimes M_z E_z{}^{n+1} \\ M_x \otimes M_y \otimes A_z E_x{}^{n+1} \\ A_x \otimes M_y \otimes M_z E_y{}^{n+1} \end{bmatrix}, \tag{32}$$

where M^x, M^y, M^z are 1D mass matrices, S^x, S^y, S^z are 1D stiffness matrices, and A_x, A_y, A_z are 1D advection matrices.

We discover the Kronecker product matrices on the left-hand sides, which can be factorized in a linear cost

$$\begin{bmatrix} M_x \otimes \left(M_y + \frac{\tau^2}{4\varepsilon\mu} S_y\right) \otimes M_z E_x{}^{n+\frac{1}{2}} \\ M_x \otimes M_y \otimes \left(M_z + \frac{\tau^2}{4\varepsilon\mu} S_z\right) E_y{}^{n+\frac{1}{2}} \\ \left(M_x + \frac{\tau^2}{4\varepsilon\mu} S_x\right) \otimes M_y \otimes M_z E_z{}^{n+\frac{1}{2}} \end{bmatrix} = \mathscr{R}\mathscr{H}\mathscr{S}, \tag{33}$$

$$\begin{bmatrix} M_x \otimes M_y \otimes M_z H_x{}^{n+\frac{1}{2}} \\ M_x \otimes M_y \otimes M_z H_y{}^{n+\frac{1}{2}} \\ M_x \otimes M_y \otimes M_z H_z{}^{n+\frac{1}{2}} \end{bmatrix} = \mathscr{R}\mathscr{H}\mathscr{S}, \tag{34}$$

$$\begin{bmatrix} M_x \otimes M_y \otimes \left(M_z + \frac{\tau^2}{4\varepsilon\mu} S_z\right) E_x{}^{n+1} \\ \left(M_x + \frac{\tau^2}{4\varepsilon\mu} S_x\right) \otimes M_y \otimes M_z E_y{}^{n+1} \\ M_x \otimes \left(M_y + \frac{\tau^2}{4\varepsilon\mu} S_y\right) \otimes M_z E_z{}^{n+1} \end{bmatrix} = \mathscr{R}\mathscr{H}\mathscr{S}, \tag{35}$$

$$\begin{bmatrix} M_x \otimes M_y \otimes M_z H_x{}^{n+1} \\ M_x \otimes M_y \otimes M_z H_y{}^{n+1} \\ M_x \otimes M_y \otimes M_z H_z{}^{n+1} \end{bmatrix} = \mathscr{R}\mathscr{H}\mathscr{S}. \tag{36}$$

3.3. Varying material data for Maxwell equations

Let us explain the idea of varying material data coefficients using the first system of equations, in the weak form, solved in the even sub-steps, to update the electric field. For other systems, the idea is identical. In the problem matrix, for the even sub-steps, for the electric field computations, we have

$$\begin{bmatrix} M_x \otimes \left(M_y + \frac{\tau^2}{4\varepsilon\mu} S_y\right) \otimes M_z E_x{}^{n+\frac{1}{2}} \\ M_x \otimes M_y \otimes \left(M_z + \frac{\tau^2}{4\varepsilon\mu} S_z\right) E_y{}^{n+\frac{1}{2}} \\ \left(M_x + \frac{\tau^2}{4\varepsilon\mu} S_x\right) \otimes M_y \otimes M_z E_z{}^{n+\frac{1}{2}} \end{bmatrix} = \begin{bmatrix} M_x \otimes M_y \otimes M_z E_x{}^{n} \\ M_x \otimes M_y \otimes M_z E_y{}^{n} \\ M_x \otimes M_y \otimes M_z E_z{}^{n} \end{bmatrix} + \begin{bmatrix} -\frac{\tau}{2\varepsilon} M_x \otimes M_y \otimes A_z H_y{}^{n} \\ \frac{\tau}{2\varepsilon} M_x \otimes M_y \otimes A_z H_x{}^{n} \\ -\frac{\tau}{2\varepsilon} M_x \otimes A_y \otimes M_z H_x{}^{n} \end{bmatrix} + \begin{bmatrix} \frac{\tau}{2\varepsilon} M_x \otimes A_y \otimes M_z H_z{}^{n} \\ -\frac{\tau}{2\varepsilon} A_x \otimes M_y \otimes M_z H_z{}^{n} \\ -\frac{\tau}{2\varepsilon} M_x \otimes A_y \otimes A_x \otimes M_y \otimes M_z H_y{}^{n} \end{bmatrix} + \begin{bmatrix} \frac{\tau^2}{4\varepsilon\mu} A_x \otimes A_y \otimes M_z E_y{}^{n} \\ \frac{\tau^2}{4\varepsilon\mu} M_x \otimes A_y \otimes A_z E_z{}^{n} \\ \frac{\tau^2}{4\varepsilon\mu} A_x \otimes M_y \otimes M_z E_x{}^{n} \end{bmatrix}$$

where M_x, M_y, M_z are 1D mass matrices, S_x, S_y, S_z are 1D stiffness matrices, and A_x, A_y, A_z are 1D advection matrices. Rewriting the equations in the matrix form with the B-spline functions for trial and testing, we have

$$\mathscr{M}_1^1 E_x{}^{n+\frac{1}{2}} = \mathscr{M}_1 E_x{}^{n} + \mathscr{F}_1^1 H_y{}^{n} + \mathscr{F}_1^2 H_z{}^{n} + \mathscr{F}_1^3 E_y{}^{n} = \mathscr{R}\mathscr{H}\mathscr{S}_1,$$
$$\mathscr{M}_2^1 E_y{}^{n+\frac{1}{2}} = \mathscr{M}_2 E_y{}^{n} + \mathscr{F}_2^1 H_x{}^{n} + \mathscr{F}_2^2 H_z{}^{n} + \mathscr{F}_2^3 E_z{}^{n} = \mathscr{R}\mathscr{H}\mathscr{S}_2,$$
$$\mathscr{M}_3^1 E_z{}^{n+\frac{1}{2}} = \mathscr{M}_3 E_z{}^{n} + \mathscr{F}_3^1 H_x{}^{n} + \mathscr{F}_3^2 H_y{}^{n} + \mathscr{F}_3^3 E_x{}^{n} = \mathscr{R}\mathscr{H}\mathscr{S}_3,$$

$$\mathscr{M}^1_{1\,ijk,lmo} = \int_{\Omega_x} B_i^x B_l^x \,\mathrm{d}x \int_{\Omega_y} \left(B_j^y B_m^y + \frac{\tau^2}{4\varepsilon\mu} \frac{\partial B_j^y}{\partial y} \frac{\partial B_m^y}{\partial y}\right) \mathrm{d}y \int_{\Omega_z} B_k^z B_o^z \,\mathrm{d}z,$$

$$\mathscr{M}^1_{2\,ijk,lmo} = \int_{\Omega_x} B_i^x B_l^x \,\mathrm{d}x \int_{\Omega_y} B_j^y B_m^y \,\mathrm{d}y \int_{\Omega_z} \left(B_k^z B_n(z) + \frac{\tau^2}{4\varepsilon\mu} \frac{\partial B_k^z}{\partial z} \frac{\partial B_o^z}{\partial z}\right) \mathrm{d}z,$$

$$\mathscr{M}^1_{3\,ijk,lmo} = \int_{\Omega_x} \left(B^x_i B^x_l + \frac{\tau^2}{4\varepsilon\mu} \frac{\partial B^x_i}{\partial x} \frac{\partial B^x_l}{\partial x} \right) \mathrm{d}x \int_{\Omega_y} B^y_j B^y_m \,\mathrm{d}y \int_{\Omega_z} B^z_k B^z_o \,\mathrm{d}z,$$

$$\mathscr{F}^1_{1\,ijk,lmo} = -\frac{\tau}{2\varepsilon} \int_{\Omega} B^x_i B^y_j \frac{\partial B^z_k}{\partial z} B^x_l B^y_m B^z_o \,\mathrm{d}x\,\mathrm{d}y\,\mathrm{d}z,$$

$$\mathscr{F}^1_{2\,ijk,lmo} = \frac{\tau}{2\varepsilon} \int_{\Omega} B^x_i B^y_j \frac{\partial B^z_k}{\partial z} B^x_l B^y_m B^z_o \,\mathrm{d}x\,\mathrm{d}y\,\mathrm{d}z,$$

$$\mathscr{F}^1_{3\,ijk,lmo} = -\frac{\tau}{2\varepsilon} \int_{\Omega} B^x_i \frac{\partial B^y_j}{\partial y} B_k(x) B^x_l B^y_m B^z_o \,\mathrm{d}x\,\mathrm{d}y\,\mathrm{d}z,$$

t

$$\mathscr{F}^2_{1\,ijk,lmo} = \frac{\tau}{2\varepsilon} \int_{\Omega} B^x_i \frac{\partial B^y_j}{\partial y} B^x_k B^x_l B^y_m B^z_o \,\mathrm{d}x\,\mathrm{d}y\,\mathrm{d}z,$$

$$\mathscr{F}^2_{2\,ijk,lmo} = -\frac{\tau}{2\varepsilon} \int_{\Omega} \frac{\partial B^x_i}{\partial x} B^y_j B^x_k B^x_l B^y_m B^z_o \,\mathrm{d}x\,\mathrm{d}y\,\mathrm{d}z,$$

$$\mathscr{F}^2_{3\,ijk,lmo} = -\frac{\tau}{2\varepsilon} \int_{\Omega} \frac{\partial B^x_i}{\partial x} B^y_j B^x_k B^x_l B^y_m B^z_o \,\mathrm{d}x\,\mathrm{d}y\,\mathrm{d}z,$$

$$\mathscr{F}^3_{1\,ijk,lmo} = \frac{\tau^2}{4\varepsilon\mu} \int_{\Omega} \frac{\partial B^x_i}{\partial x} \frac{\partial B^y_j}{\partial y} B^x_k B^x_l B^y_m B^z_o \,\mathrm{d}x\,\mathrm{d}y\,\mathrm{d}z,$$

$$\mathscr{F}^3_{2\,ijk,lmo} = \frac{\tau^2}{4\varepsilon\mu} \int_{\Omega} B^x_i \frac{\partial B^y_j}{\partial y} B^z_k B^x_l B^y_m B^z_o \,\mathrm{d}x\,\mathrm{d}y\,\mathrm{d}z,$$

$$\mathscr{F}^3_{3\,ijk,lmo} = \frac{\tau^2}{4\varepsilon\mu} \frac{\partial B^x_i}{\partial x} B^x_k B^x_l B^y_m B^z_o \,\mathrm{d}x\,\mathrm{d}y\,\mathrm{d}z,$$

where $i = 1,\ldots,N_x$, $j = 1,\ldots,N_y$, $k = 1,\ldots,N_z$ span over the trial space dimensions, and $l = 1,\ldots,\tilde{N}_x$, $m = 1,\ldots,\tilde{N}_y$, $n = 1,\ldots,\tilde{N}_z$ span over the test space dimensions. The matrices on the right-hand side are multiplied by the solution vectors from previous time step, so as the result on the right-hand side we have a vectors $\mathscr{RHS}_{1lmo}$, $\mathscr{RHS}_{2lmo}$, and $\mathscr{RHS}_{3lmo}$, where again $l = 1,\ldots,\tilde{N}_x, m = 1,\ldots,\tilde{N}_y, o = 1,\ldots\tilde{N}_z$. The alternating-directions solver decomposes this system into the following three one-dimensional systems with multiple right-hand-sides

$$\begin{bmatrix} \mathscr{A}_1 F_1^{n+\frac{1}{2}} \\ \mathscr{A}_2 F_2^{n+\frac{1}{2}} \\ \mathscr{A}_3 F_3^{n+\frac{1}{2}} \end{bmatrix} = \begin{bmatrix} \mathscr{RHS}_1 \\ \mathscr{RHS}_2 \\ \mathscr{RHS}_3 \end{bmatrix}, \tag{37}$$

$$\begin{aligned} \mathscr{A}_{1\,i,l} &= \int_{\Omega_x} B^x_i B^x_l \,\mathrm{d}x, \quad \mathscr{A}_{2\,i,l} = \int_{\Omega_x} B^x_i B^x_l \,\mathrm{d}x, \\ \mathscr{A}_{3\,i,l} &= \int_{\Omega_x} \left(B^x_i B^x_l + \frac{\tau^2}{4\varepsilon\mu} \frac{\partial B^x_i}{\partial x} \frac{\partial B^x_l}{\partial x} \right) \mathrm{d}x \end{aligned} \tag{38}$$

and the right-hand side vectors $\mathscr{RHS}_{1\,i,jk}$, $\mathscr{RHS}_{2\,i,jk}$, $\mathscr{RHS}_{3\,i,jk}$ have been reordered into matrices with N_x rows and N_yN_z columns, by ordering blocks of N_x consecutive rows, one after another. After solving the first one-dimensional system with multiple right-hand sides we solve the second system

$$\begin{bmatrix} \mathscr{B}_1 G_1^{n+\frac{1}{2}} \\ \mathscr{B}_2 G_2^{n+\frac{1}{2}} \\ \mathscr{B}_3 G_3^{n+\frac{1}{2}} \end{bmatrix} = \begin{bmatrix} F_1^{n+\frac{1}{2}} \\ F_2^{n+\frac{1}{2}} \\ F_3^{n+\frac{1}{2}} \end{bmatrix}, \tag{39}$$

$$\mathscr{B}_{1\,j,m} = \int_{\Omega_y} \left(B^y_j B^y_m + \frac{\tau^2}{4\varepsilon\mu} \frac{\partial B^y_j}{\partial y} \frac{\partial B^y_m}{\partial y} \right) \mathrm{d}y,$$

$$\mathscr{B}_{2\,j,m} = \int_{\Omega_y} B^y_j B^y_m \,\mathrm{d}y, \quad \mathscr{B}_{3\,j,m} = \int_{\Omega_y} B^y_j B^y_m \,\mathrm{d}y.$$

We solve the third system with multiple right-hand sides

$$\begin{bmatrix} \mathscr{C}_1 E_x{}^{n+\frac{1}{2}} \\ \mathscr{C}_2 E_y{}^{n+\frac{1}{2}} \\ \mathscr{C}_3 E_z{}^{n+\frac{1}{2}} \end{bmatrix} = \begin{bmatrix} G_1^{n+\frac{1}{2}} \\ G_2^{n+\frac{1}{2}} \\ G_3^{n+\frac{1}{2}} \end{bmatrix}, \tag{40}$$

$$\mathscr{C}_{1\,k,o} = \int_{\Omega_z} B^z_k B^z_o dz \quad \mathscr{C}_{3\,k,o} = \int_{\Omega_z} B^z_k B^z_o \,\mathrm{d}z,$$

$$\mathscr{C}_{2\,k,o} = \int_{\Omega_z} \left(B^z_k B^z_o + \frac{\tau^2}{4\varepsilon\mu} \frac{\partial B^z_k}{\partial z} \frac{\partial B^z_o}{\partial z} \right) \mathrm{d}z.$$

We assign different material data to different B-splines used for testing our equation. Since each test B-spline results in a single equation in the global system of equations, we localize this equation in the three systems with multiple right-hand sides. Having the equations identified, we modify the material data in the three systems of equations as processed by the alternating directions solver. We modify material data $\varepsilon = \hat{\varepsilon}$, $\mu = \hat{\mu}$ for test B-spline "rst", namely $B_r(x)B_s(y)B_t(z)$. the limitation of our method is that we can only provide one value of the material data coefficients for a single test function. Thus, the material data coefficients are averaged with the distributions prescribed by test functions. When we employ B-spline basis functions, as they preserve the partition of unity property, the distributions of material data averaged with overlapping B-spline test functions; they sum up to one. To introduce the averaged material data coefficients $\varepsilon = \hat{\varepsilon}$, $\mu = \hat{\mu}$, we perform the following changes. In the first system, we extract the three equations (three rows) for the three components of the electric field for row $i = r$, and the suitable columns from the right-hand side $l = r, m = s, o = t$, where we modify material data

$$\sum_{l=1,\ldots,N_x} \int_{\Omega_x} B_r(x) B^x_l dx * F_1^{n+\frac{1}{2}}{}_{lst} = \mathscr{R}\hat{\mathscr{H}}\mathscr{S}_{1rst}, \tag{41}$$

$$\sum_{l=1,\ldots,N_x} \int_{\Omega_x} B_r(x) B^x_l dx * F_2^{n+\frac{1}{2}}{}_{lst} = \mathscr{R}\hat{\mathscr{H}}\mathscr{S}_{2rst}, \tag{42}$$

$$\sum_{l=1,\ldots,N_x}\int_{\Omega_x}\left(B_r(x)B_l^x+\frac{\hat{\tau}^2}{4\hat{\varepsilon}\hat{\mu}}\frac{\partial B_r(x)}{\partial x}\frac{\partial B_l^x}{\partial x}\right)\mathrm{d}x$$

$$*F_3^{n+\frac{1}{2}}{}_{lst}=\mathscr{R}\hat{\mathscr{H}}\mathscr{S}_{3rst}\,. \tag{43}$$

The $\mathscr{R}\hat{\mathscr{H}}\mathscr{S}_{1rst}$, $\mathscr{R}\hat{\mathscr{H}}\mathscr{S}_{2rst}$, $\mathscr{R}\hat{\mathscr{H}}\mathscr{S}_{3rst}$ represent the right-hand sides with material data parameters $\varepsilon=\hat{\varepsilon}$, $\mu=\hat{\mu}$. The other rows and columns in the first system remain unchanged.

Similarly, in the second system, we extract the equation for row $j=s$ and columns $l=r$, $m=s$, $n=t$

$$\sum_{m=1,\ldots,N_y}\int_{\Omega_y}\left(B_s(y)B_m^y+\frac{\hat{\tau}^2}{4\hat{\varepsilon}\hat{\mu}}\frac{\partial B_s(y)}{\partial y}\frac{\partial B_m^y}{\partial y}\right)\mathrm{d}y$$

$$*G_1^{n+\frac{1}{2}}{}_{rmt}=F_1^{n+\frac{1}{2}}{}_{rst}\,, \tag{44}$$

$$\sum_{m=1,\ldots,N_y}\int_{\Omega_y}B_s(y)B_m^y\,\mathrm{d}y\quad *G_2^{n+\frac{1}{2}}{}_{rmt}=F_2^{n+\frac{1}{2}}{}_{rst}\,, \tag{45}$$

$$\sum_{m=1,\ldots,N_y}\int_{\Omega_y}B_s(y)B_m^y\,\mathrm{d}y\quad *G_3^{n+\frac{1}{2}}{}_{rmt}=F_3^{n+\frac{1}{2}}{}_{rst} \tag{46}$$

and we modify the material data. The other rows and columns remain unchanged. In the third system, we extract the equation for row $k=t$ and columns $l=r$, $m=s$, $n=t$

$$\sum_{o=1,\ldots,N_z}\int_{\Omega_z}B_t(z)B_o^z\,\mathrm{d}z*E_x{}^{n+\frac{1}{2}}{}_{rso}=G_1^{n+\frac{1}{2}}{}_{rst}\,, \tag{47}$$

$$\sum_{o=1,\ldots,N_z}\int_{\Omega_z}\left(B_t(z)B_o^z+\frac{\hat{\tau}^2}{4\hat{\varepsilon}\hat{m}\hat{u}}\frac{\partial B_t(z)}{\partial z}\frac{\partial B_o^z}{\partial z}\right)\mathrm{d}z$$

$$*E_z{}^{n+\frac{1}{2}}{}_{rso}=G_2^{n+\frac{1}{2}}{}_{rst}\,, \tag{48}$$

$$\sum_{o=1,\ldots,N_z}\int_{\Omega_z}B_o^zB_o^z\,\mathrm{d}z\quad *E_z{}^{n+\frac{1}{2}}{}_{rso}=G_3^{n+\frac{1}{2}}{}_{rst} \tag{49}$$

and we modify the material data. The other rows and columns in the third system remain unchanged. Similar modifications have to be performed in other sub-steps.

4. NUMERICAL RESULTS

The goal of this section is to verify the correctness of our numerical code. We first introduce a manufactured solution for the Maxwell problem. Following [1], for $\Omega=[0,1]^3$, for $\varepsilon=1$ and $\mu=1$ we define

$$u^1_{\kappa,\lambda}(x,t)=\begin{bmatrix}\sin(\kappa\pi y)\sin(\lambda\pi z)\cos(\sqrt{\kappa^2+\lambda^2}\pi t)\\0\\0\\0\\-\frac{\lambda}{\sqrt{\kappa^2+\lambda^2}}\sin(\kappa\pi y)\cos(\lambda\pi z)\sin(\sqrt{\kappa^2+\lambda^2}\pi t)\\\frac{\kappa}{\sqrt{\kappa^2+\lambda^2}}\cos(\kappa\pi y)\sin(\lambda\pi z)\sin(\sqrt{\kappa^2+\lambda^2}\pi t)\end{bmatrix},$$

$$u^2_{\kappa,\lambda}(x,t)=\begin{bmatrix}0\\\sin(\kappa\pi x)\sin(\lambda\pi z)\cos(\sqrt{\kappa^2+\lambda^2}\pi t)\\0\\\frac{\lambda}{\sqrt{\kappa^2+\lambda^2}}\sin(\kappa\pi x)\cos(\lambda\pi z)\sin(\sqrt{\kappa^2+\lambda^2}\pi t)\\0\\-\frac{\kappa}{\sqrt{\kappa^2+\lambda^2}}\cos(\kappa\pi x)\sin(\lambda\pi z)\sin(\sqrt{\kappa^2+\lambda^2}\pi t)\end{bmatrix},$$

$$u^3_{\kappa,\lambda}(x,t)=\begin{bmatrix}0\\0\\\sin(\kappa\pi x)\sin(\lambda\pi y)\cos(\sqrt{\kappa^2+\lambda^2}\pi t)\\-\frac{\lambda}{\sqrt{\kappa^2+\lambda^2}}\sin(\kappa\pi x)\cos(\lambda\pi y)\sin(\sqrt{\kappa^2+\lambda^2}\pi t)\\\frac{\kappa}{\sqrt{\kappa^2+\lambda^2}}\cos(\kappa\pi x)\sin(\lambda\pi y)\sin(\sqrt{\kappa^2+\lambda^2}\pi t)\\0\end{bmatrix}$$

for $\kappa,\lambda\in\mathscr{N},\kappa,\lambda\neq 0$.

Using these function, we can define manufactured solutions for the non-stationary Maxwell problem. One of the solution for $\kappa=1$, $\lambda=1$ can be introduced as

$$\mathbf{u}_A(x,t)=\gamma u^1_{1,1}(x,t)+2\gamma u^2_{1,1}(x,t)+3\gamma u^3_{1,1}(x,t). \tag{50}$$

Notice that $\mathbf{u}_A$ has six components, where the first three components denote the electric field $\mathbf{E}$ and the last three components denote the magnetic field $\mathbf{H}$. The parameter γ is selected in such a way thats $\|\mathbf{u}_A(x,0)\|_{L^2(\Omega)}=1$. In the code, we solve

$$\frac{\partial\mathbf{E}}{\partial t}(t)=\frac{1}{\varepsilon}\nabla\times\mathbf{H}(t)\quad t\in\mathscr{R},\ \ x\in\Omega, \tag{51}$$

$$\frac{\partial\mathbf{H}}{\partial t}(t)=-\frac{1}{\mu}\nabla\times\mathbf{E}(t)\quad t\in\mathscr{R},\ \ x\in\Omega, \tag{52}$$

$$\mathrm{div}\varepsilon\mathbf{E}(t)=0\quad t\in\mathscr{R},\ \ x\in\Omega, \tag{53}$$

$$\mathrm{div}\mu\mathbf{H}(t)=0\quad t\in\mathscr{R},\ \ x\in\Omega, \tag{54}$$

$$\mathbf{E}(t)\times\mathbf{n}=0\quad t\in\mathscr{R},\ \ x\in\partial\Omega, \tag{55}$$

$$\mathbf{H}(t)\cdot\mathbf{n}=0\quad t\in\mathscr{R},\ \ x\in\partial\Omega, \tag{56}$$

$$\mathbf{E}(x,0)=\mathbf{E_0}(x)\quad x\in\Omega, \tag{57}$$

$$\mathbf{H}(x,0)=\mathbf{H_0}(x)\quad x\in\Omega. \tag{58}$$

The initial states $\mathbf{E_0}$ and $\mathbf{H_0}$ are selected using $u_A(x,0)$, the permittivity $\varepsilon=1$, and the permeability $\mu=1$.

Next, we introduce non-regular material data representing the human head. In other words, we put the human head into this electromagnetic field and observe the result. Our simulations are based on digital data, the MRI scan with 29 two-dimensional slices, each one with 532 times 565 pixels. Each pixel intensity is a value from the range of [0, 255], and it is proportional to the material (skull, skin, tissue, and air) normalized density. Exemplary slices of the human head from the MRI scan are presented in Fig. 2. Next, according to the MRI scan data, we employ material data changing on the skull, skin, tissue, and air. We assume air (MRI scan data ≤ 1), skin or brain (tissue in general) ($1 \leq$ approximation ≤ 240), and skull (approximation ≥ 240). We enforce different material data using the method described in this section. The material data in the Maxwell equations are selected according to the tissue kind, following [16]. Namely, we introduce $\hat{\varepsilon} \in \{\hat{\varepsilon}_{\text{AIR}}, \hat{\varepsilon}_{\text{TISSUE}}, \hat{\varepsilon}_{\text{BONE}}\} = \{1.0, 45.8, 16.6\}$ and $\hat{\mu} = \{\hat{\mu}_{\text{AIR}}, \hat{\mu}_{\text{TISSUE}}, \hat{\mu}_{\text{BONE}}\} = \{1.0, 1.0, 1.0\}$. The material data $\hat{\varepsilon}, \hat{\mu}$ are defined as relative to the vacuum permittivity and permeability of free space, namely $\varepsilon = \hat{\varepsilon}\varepsilon_0$, where $\varepsilon_0 = 8.854 \times 10^{-12}$, and $\mu = \hat{\mu}\mu_0$, where $\mu_0 = 12.556 \times 10^{-7}$. The permeability μ, as related to a magnetic field, is not sensitive to varying materials. Thus, all its components are equal.

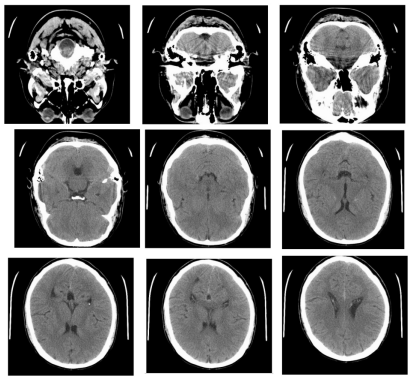

Fig. 2. Exemplary cross-sections of the MRI scans of the human head

We investigate now the obtained numerical results. In Fig. 3, we present the snap shoot from the simulation – the configuration of the electric and magnetic fields, obtained from this

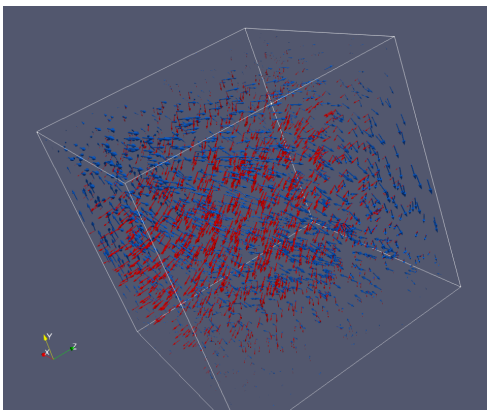

Fig. 3. Electric (red) and magnetic (blue) vector fields, resulting from the problem with manufactured solution

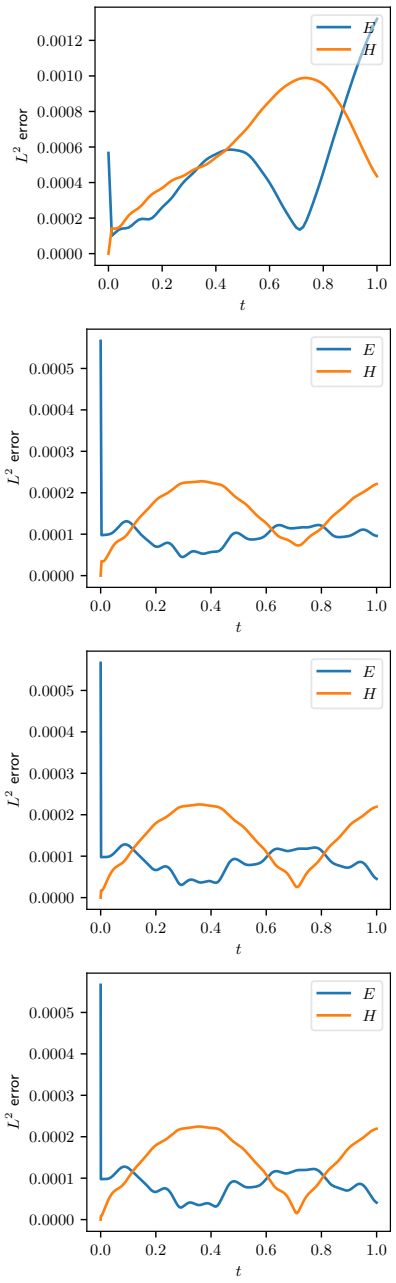

Fig. 4. L2 norm error of electric (blue) and magnetic (orange) vector fields resulting from the solution of the problem with manufactured solution over the mesh with $16 \times 16 \times 16$ elements, for the time interval [0, 1], with number of time steps within [0, 1] interval varying from 80 (first row), 320 (second row), 640 (third row), and 1280 (last row)

manufactured solution. In Fig. 6 we present the percentage of the relative L^2 norm error between the numerical and analytical solutions computed for the entire time-interval of the simulation, with different time steps, with $16 \times 16 \times 16$ mesh. Namely, we compute

$$\text{Electric field } L_2 \text{ error} = 100 \times \int_0^1 \frac{\|E_{\text{exact}}(x,y,z;t) - E(x,y,z;t)\|_{L^2(\Omega)}}{\|E_{\text{exact}}(x,y,z;t)\|_{L^2(\Omega)}} \, \mathrm{d}t, \qquad (59)$$

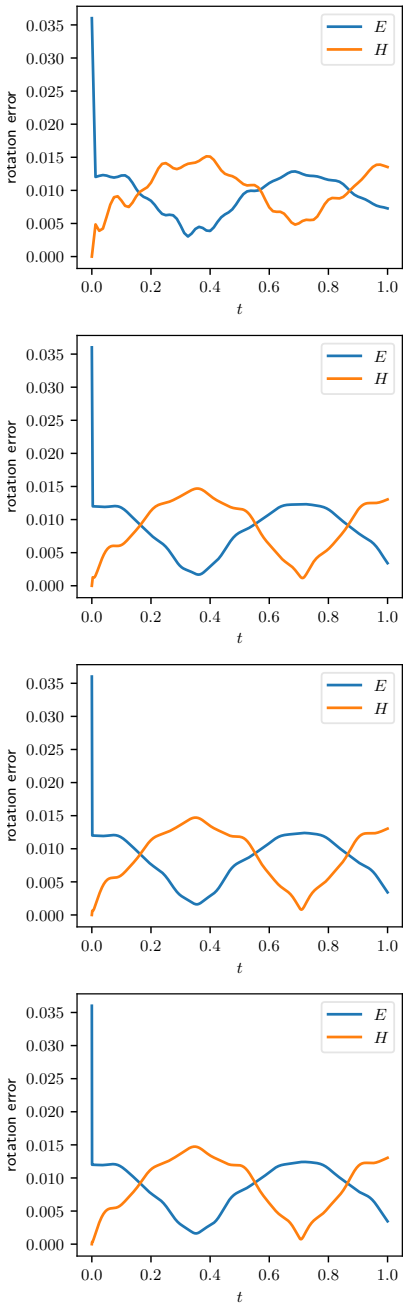

Fig. 5. H-curl norm error of electric (blue) and magnetic (orange) vector fields resulting from the solution of the problem with manufactured solution over the computational mesh with $16\times16\times16$ elements, for the time interval $[0, 1]$, with number of time step varying from 80 (first row), 320 (second row), 640 (third row), and 1280 (last row)

Magnetic field L_2 error =

$$100\times\int_0^1 \frac{\|H_{\text{exact}}(x,y,z;t)-H(x,y,z;t)\|_{L^2(\Omega)}}{\|H_{\text{exact}}(x,y,z;t)\|_{L^2(\Omega)}}\,\mathrm{d}t. \quad (60)$$

In Fig. 7 we present the percentage of the relative $H(\text{curl})$ norm error between the numerical and analytical solutions computed for the entire time interval of the simulation, with different time steps.

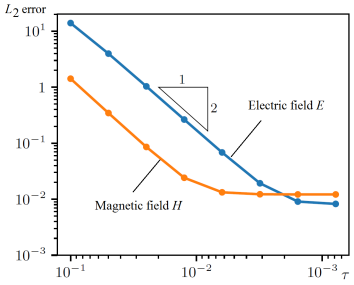

Fig. 6. Percentage of the L^2 relative error between computed electric (red) or magnetic (blue) vector fields, and the exact solution of the manufactured problem

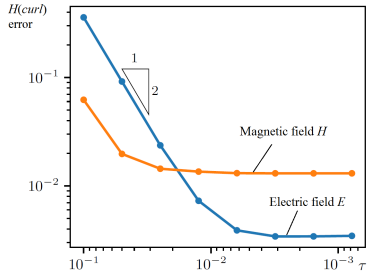

Fig. 7. Percentage of the $H(curl)$ relative error between computed electric (red) or magnetic (blue) vector fields, and the exact solution of the manufactured problem

Electric field $H(\text{curl})$ error =

$$100\times\int_0^1 \frac{\|E_{\text{exact}}(x,y,z;t)-E(x,y,z;t)\|_{H(\text{curl})(\Omega)}}{\|E_{\text{exact}}(x,y,z;t)\|_{H(curl)(\Omega)}}\,\mathrm{d}t, \quad (61)$$

Magnetic field $H(\text{curl})$ error =

$$=100\times\int_0^1 \frac{\|H_{\text{exact}}(x,y,z;t)-H(x,y,z;t)\|_{H(\text{curl})(\Omega)}}{\|H_{\text{exact}}(x,y,z;t)\|_{H(\text{curl})(\Omega)}}\,\mathrm{d}t. \quad (62)$$

From these experiments, we can conclude that our time-integration scheme, including the operator splitting, is second-order accurate in time (one-order decrease of the time step size results in two-order of magnitude lower error), and it provides correct numerical solutions. Further increase in the accuracy would require increasing of the spatial mesh dimensions.

In Fig. 4, we investigate the convergence of the solution measured in L^2 norm when we increase the number of time steps, from $\frac{1}{80}=0.0125$, $\frac{1}{320}=.0.003125$, $\frac{1}{640}=0.0015625$, and $\frac{1}{1280}=0.00078125$. In other words, we decrease the time step size, and observe the numerical accuracy. Similarly, in Figs. 5, we investigate the convergence in the $H-curl$ norm when increasing the number of time steps (decreasing the time step size). We can see that the numerical error becomes stable during the entire simulation, and it does not grow with time steps more than 0.0002 for the L^2 norm and more than 0.015 for the $H-\text{curl}$ norm for the smallest time step size employed. We conclude that the method is stable and convergent.

Finally, we summarize the results of propagation of electromagnetic waves on the human head in Figs. 8–9. We can see the interaction of the electromagnetic field with the human head, as well as with the metallic handle, employed the keep the human head stable during the MRI procedure.

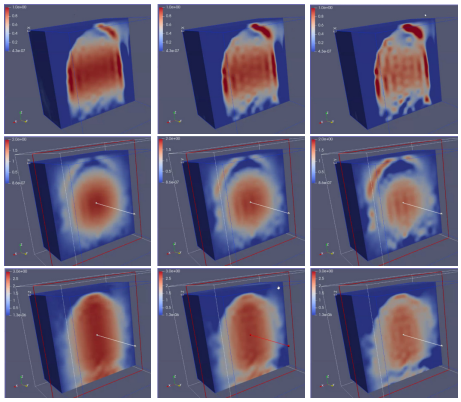

Fig. 8. First row: x component of the electric vector field. Second row: y component of the electric vector field. Third row: z component of the electric vector field. Columns – cross section along OYZ plane, time moments: 0, 0.25, 0.5, 0.75, 1.0s. $32\times32\times32$, quadratic C^1 B-splines

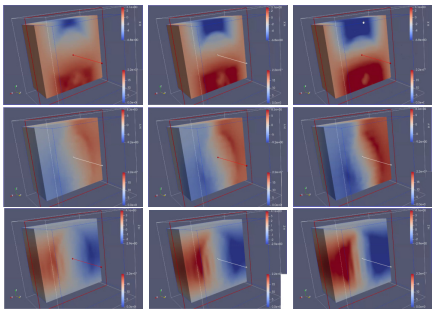

Fig. 9. First row: x component of the magnetic vector field. Second row: y component of the magnetic vector field. Third row: z component of the magnetic vector field. Columns – cross section along OYZ plane, time moments: 0, 0.25, 0.5, 0.75, 1.0 s. $32\times32\times32$, quadratic C^1 B-splines

5. SCALABILITY OF THE PARALLEL SHARED-MEMORY CODE

In this section, we present the measurements of the execution time of the parallel shared-memory code for non-stationary Maxwell simulations with non-constant material data. We implemented our method in [15] framework. The experiments were performed on a Linux workstation equipped with AMD Ryzen 9 3900X processor with 12 physical cores and a total of 24 virtual cores, with 64 GB of RAM. We run the measurements for linear, quadratic, and cubic B-splines for $8\times8\times8$, $32\times32\times32$, and $128\times128\times128$ elements. The execution times are summarized in Tables 1–3. We verify now a linear computational cost for different numbers of processors and orders of B-splines. We measure the time per element, measured in nano-seconds per element, where we increase the number of elements. We perform these measurements for one core and for 24 cores. We can see from Fig. 10–11 that the execution time per element remains constant when we increase the mesh from $8\times8\times8=512$ to $128\times128\times128=2\,097\,152$ elements. We conclude that our code delivers a linear computational cost. We also measure the speedup for computational grids of size $32\times32\times32$ and $128\times128\times128$, and we summarize the experiments in Tables 2–4. In Tables 2 and 4, we can observe that speedup grows beyond the number of physical cores. As it is true, please note that after reaching 12 cores, speedup growth is slightly flatter. The main reason is that Hyper-threading (HT) technology is more mature than several years ago. Also, the type of workload considered in this paper benefits from HT. Hyper-threading allows a single physical core to execute multiple threads simultaneously. The physical core can only execute one instruction at a time. HT

Table 1

Execution time (time [s]) over the $32\times32\times32$ mesh, with linear ($p=1$), quadratic ($p=2$), and cubic ($p=3$) B-splines, with number of cores varying from 1 to 24

# cores	p_1	p_2	p_3
1	6.02	65.05	358.18
2	3.11	33.24	183.03
4	1.59	16.81	92.27
8	0.85	8.79	48.68
12	0.58	6.00	33.04
16	0.51	4.96	26.38
24	0.38	3.59	19.54

Table 2

Speedup over the $32\times32\times32$ mesh, with linear ($p=1$), quadratic ($p=2$), and cubic ($p=3$) B-splines, with number of cores varying from 1 to 24

# cores	p_1	p_2	p_3
1	1	1	1
2	1.93	1.95	1.95
4	3.77	3.86	3.88
8	7.06	7.39	7.35
12	10.28	10.83	10.83
16	11.72	13.10	13.57
24	15.66	18.07	18.32

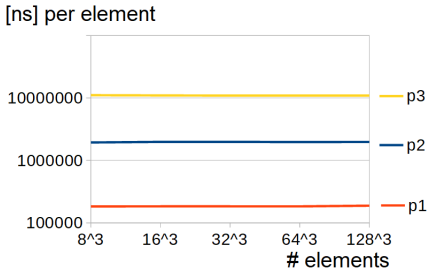

Fig. 10. Time [ns] per element. Number of elements from $8\times8\times8=512$ to $128\times128\times128=2\,097\,152$ elements. Measurements for linear ($p=1$), quadratic ($p=2$), cubic ($p=3$) B-splines, with 1 core

allows the CPU core to switch between multiple threads quickly. This is highly beneficial when one thread waits for data from RAM or another resource. The core can switch to another thread that is ready to execute. Please note that the speedup achieved by Hyper-threading depends on the nature of the workload.

Table 3

Execution time [s] over $128 \times 128 \times 128$ mesh, linear ($p = 1$), quadratic ($p = 2$), and cubic ($p = 3$) B-splines, # cores from 1 to 24

# cores	p_1	p_2	p_3
1	395.21	4152.44	22935.37
2	203.69	2113.76	11830.60
4	104.10	1082.28	5987.16
8	55.06	566.83	3151.49
12	38.07	383.91	2133.77
16	34.28	330.98	1810.17
24	25.75	238.18	1275.99

Table 4

Speedup over $128 \times 128 \times 128$ mesh, with linear ($p = 1$), quadratic ($p = 2$), and cubic ($p = 3$) B-splines, # cores from 1 to 24

# cores	p_1	p_2	p_3
1	1	1	1
2	1.94	1.96	1.93
4	3.79	3.83	3.83
8	7.17	7.32	7.27
12	10.38	10.81	10.74
16	11.52	12.54	12.67
24	15.34	17.43	17.97

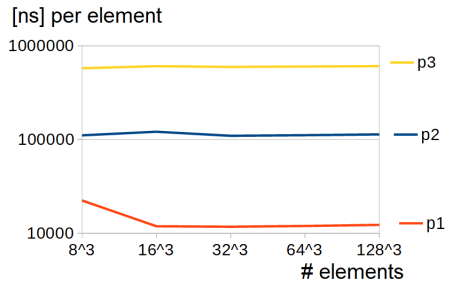

Fig. 11. Time [ns] per element. Number of elements from $8 \times 8 \times 8 = 512$ to $128 \times 128 \times 128 = 2\,097\,152$ elements. Measurements for linear ($p = 1$), quadratic ($p = 2$), cubic ($p = 3$) B-splines, with 24 cores

6. CONCLUSIONS

We show that it is possible to vary material data in non-stationary Maxwell simulations, preserving the linear computational cost of the direction splitting solver. In our method we can vary the material data with test functions. We test the method using the model Maxwell problem formulation and we put the non-regular material data obtained from the MRI scan.

ACKNOWLEDGEMENTS

Research project supported by the program "Excellence initiative – research university" for the AGH University of Krakow.

REFERENCES

[1] M. Hochbruck, T. Jahnke, and R. Schnaubelt, "Convergence of an ADI splitting for Maxwell's equations," *Numer. Math.*, vol. 129, pp. 535–561, 2015.

[2] J.A. Cottrell, T.J.R. Hughes, and Y. Bazilevs, *Isogeometric Analysis: Towards Unification of Computer Aided Design and Finite Element Analysis* John Wiley and Sons, 2009.

[3] D.W. Peaceman and H.H. Rachford Jr., "The numerical solution of parabolic and elliptic differential equations," *J. Soc. Ind. Appl. Math.*, vol. 3, pp. 28–41, 1955.

[4] J. Douglas and H. Rachford, "On the numerical solution of heat conduction problems in two and three space variables," *Trans. Am. Math. Soc.*, vol. 82, pp. 421–439, 1956.

[5] G.I. Marchuk, "Splitting and alternating direction methods," *Handbook of numerical analysis.* Elsevier, 1990, vol. 1, pp. 197–462.

[6] P.N. Vabishchevich, *Additive operator-difference schemes: Splitting schemes.* Walter de Gruyter, 2013.

[7] P. Behnoudfar, V.M. Calo, Q. Deng, and P.D. Minev, "A variationally separable splitting for the generalized-α method for parabolic equations," *Int. J. Numer. Methods Eng.*, vol. 121, no 5, pp. 828–841, 2020.

[8] G. Liping, "Stability and Super Convergence Analysis of ADI-FDTD for the 2D Maxwell Equations in a Lossy Medium," *Acta Math. Sci.*, vol. 32, no. 6, pp. 2341–2368, 2012.

[9] J. Keating and P. Minev, "A fast algorithm for direct simulation of particulate flows using conforming grids," *J. Comput. Phys.*, vol. 255, pp. 486–501, 2013.

[10] L. Gao and V. Calo, "Fast isogeometric solvers for explicit dynamics," *Comput. Meth. Appl. Mech. Eng.*, vol. 274, pp. 19–41, 2014.

[11] L. Gao and V. Calo, "Preconditioners based on the alternating-direction-implicit algorithm for the 2d steady-state diffusion equation with orthotropic heterogeneous coefficients," *J. Comput. Appl. Math.*, vol. 273, pp. 274–295, 2015.

[12] M. Łoś, M. Paszyński, A. Kłusek, and W. Dzwinel, "Application of fast isogeometric l2 projection solver for tumor growth simulations," *Comput. Meth. Appl. Mech. Eng.*, vol. 316, pp. 1257–1269, 2017.

[13] M. Łoś, M. Woźniak, M. Paszyński, L. Dalcin, and V. Calo, "Dynamics with matrices possessing Kronecker product structure," *Procedia Comput. Sci.*, vol. 51, pp. 286–295, 2015.

[14] M. Łoś *et al.*, "Fast parallel IGA-ADS solver for time-dependent Maxwell's equations," *Comput. Math. Appl.*, vol. 151, pp. 36–49, 2023.

[15] M. Łoś, M. Woźniak, M. Paszyński, A. Lenharth, and K. Pingali, "IGA-ADS: Isogeometric Analysis FEM using ADS solver," *Comput. Phys. Commun.*, vol. 217, pp. 99–116, 2017.

[16] K. Kyunogjoo, "Finite element modeling of the radiation and induced heat transfer in the human body," Ph.D. dissertation, The University of Texas at Austin, 2013.